HHS Public Access

Author manuscript

Biochemistry. Author manuscript; available in PMC 2015 November 24.

Published in final edited form as:

Biochemistry. 2013 November 19; 52(46): 8352–8362. doi:10.1021/bi400824x.

CNG channel subunit glycosylation regulates MMP-dependent changes in channel gating

Starla E. Meighan, **Peter C. Meighan**, **Elizabeth D. Rich**, **R. Lane Brown**[1], and **Michael D. Varnum**[2,*]

Dept. of Integrative Physiology and Neuroscience, Program in Neuroscience, Washington State University, P.O. Box 647620, Pullman, WA 99164

[1]WWAMI Medical Education Program, Washington State University, P.O. Box 647620, Pullman, WA 99164

[2]Center for Integrated Biotechnology, Washington State University, P.O. Box 647620, Pullman, WA 99164

Abstract

Cyclic-nucleotide gated (CNG) channels are essential for phototransduction within retinal photoreceptors. We have demonstrated previously that enzymatic activity of matrix metalloproteinase-2 and -9, members of the MMP family of extracellular, Ca^{+2}- and Zn^{+2}-dependent proteases, enhances the ligand sensitivity of both rod (CNGA1 + CNGB1) and cone CNGA3 + CNGB3) CNG channels. Additionally, we have observed a decrease in maximal CNG channel current (I_{MAX}) that begins late during MMP-directed gating changes. Here we demonstrate that CNG channels become non-conductive after prolonged MMP exposure. Concurrent with the loss of conductive channels is the increased relative contribution of channels exhibiting non-modified gating properties, suggesting the presence of a subpopulation of channels that are protected from MMP-induced gating effects. CNGA subunits are known to possess one extracellular core glycosylation site, located at one of two possible positions within the turret loop near the pore-forming region. Our results indicate that CNGA glycosylation can impede MMP-dependent modification of CNG channels. Furthermore, the relative position of the glycosylation site within the pore turret influences the extent of MMP-dependent proteolysis. Glycosylation at the site found in CNGA3 subunits was found to be protective, while glycosylation at the bovine CNGA1 site was not. Relocating the glycosylation site in CNGA1 to the position found in CNGA3 recapitulated CNGA3-like protection from MMP-dependent processing. Taken together, these data indicate that CNGA glycosylation may protect CNG channels from MMP-dependent proteolysis, consistent with MMP modification of channel function having a requirement for physical access to the extracellular face of the channel.

*To whom correspondence should be addressed: Michael D. Varnum, Dept. of Integrative Physiology and Neuroscience, Washington State University, P.O. Box 647620, Pullman, WA, 99164, USA; Tel.: (509) 335-0661, Fax: (509) 335-4650; varnum@wsu.edu.

INTRODUCTION

Cyclic nucleotide gated (CNG) channels are members of the voltage-gated channel superfamily and are activated by the intracellular binding of cyclic nucleotides. In the visual system, CNG channels are the principal ion channels responsible for transduction of a light-induced decrease in intracellular cGMP into a photoreceptor electrical response. Native photoreceptor CNG channels are hetero-tetrameric proteins composed of two structurally related subunit types: CNGA1 and CNGB1 in rod photoreceptors; CNGA3 and CNGB3 in cone photoreceptors.[1,2] The sensitivity of CNG channels to their endogenous ligands—cGMP and cAMP—is regulated by various *intracellular* effectors,[3] including calcium-sensor proteins,[4,5] serine/threonine and tyrosine kinases[6–8] and phosphoinositides.[9–12] The altered channel gating properties produced by these regulatory inputs is thought to contribute to light/dark adaptation,[3,13] and paracrine and circadian control of photoreceptor sensitivity.[14,15]

We have recently demonstrated that CNG channel function can be influenced by members of a family of secreted endopeptidases, matrix metalloproteinases (MMPs), via proteolytic modification of CNGA subunits.[16] For both heterologously-expressed and native CNG channels, extracellular exposure to MMPs dramatically increased the apparent affinity for cGMP and the efficacy of cAMP. The gating changes with MMPs occurred more rapidly when the channels were mostly closed compared to channels held open in a saturating concentration of cGMP, suggesting state-dependent exposure of critical extracellular regions. These findings highlighted potential *extracellular* control of channel ligand sensitivity. Given that MMP modifications profoundly alter the ligand sensitivity of CNG channels, we predicted that other extracellular features might regulate processing of channels by MMPs. CNGA subunits typically possess a single, extracellular glycosylation site within the pore-turret loop. Glycosylation is well characterized as a critical factor for maturation, trafficking, and stability of membrane proteins,[17–20] and can also influence protein activity.[21,22] However, it has been demonstrated previously that the absence of the CNGA pore-turret glycosylation has no apparent effect on the functional expression or gating properties of CNG channels.[23,24] Thus, the functional importance of CNGA subunit glycosylation has remained elusive.

We hypothesized that CNGA pore-turret glycosylation decreases susceptibility to extracellular subunit proteolysis—providing protection from MMP-dependent gating changes. Here we demonstrate that a subpopulation of channels composed of CNGA subunits, with or without CNGB subunits, is protected from MMP-dependent proteolysis. Protection from MMP-mediated processing was observed for both heterologously expressed and native retinal CNG channels. We show that channel protection is primarily due to glycosylation in the CNGA pore turret, and is dependent on the location of the glycosylation site within the turret. These findings suggest that the conserved CNG channel pore-turret glycosylation modulates MMP-dependent regulation of CNG channel gating.

EXPERIMENTAL PROCEDURES

Molecular biology and functional expression

For heterologous expression in *Xenopus laevis* oocytes, the coding sequence for human CNGA3[25] was engineered to have an amino-terminal 3X-FLAG epitope tag.[26] The human CNGB3 clone was isolated previously from human retinal cDNA.[27] FLAG-tagged bovine CNGA1 was generated as previously described.[26] HA-tagged human CNGB1 was a generous gift from Dr. S.E. Gordon. All channel cDNAs were subcloned previously into pGEMHE. Site-directed mutagenesis of CNGA3 and CNGA1 was carried out as previously described.[27] Oocytes were isolated and microinjected with ~5 ng of mRNA (for all constructs). For efficient generation of heteromeric channels, the ratio of CNGA mRNA to CNGB mRNA was 1:2.5.[26] Oocytes were incubated in ND96 (96 mM NaCl, 2 mM KCl, 1.8 mM $CaCl_2$, 1 mM $MgCl_2$, and 5 mM HEPES, pH 7.6, supplemented with 10 μg/ml gentamycin) at a temperature of 17–19 °C.

Electrophysiology

One to 7 days after microinjection of mRNA, patch-clamp experiments were performed in the inside-out configuration. Recordings were made at 20–23 °C. Voltage control was provided by an Axopatch 200B amplifier (Molecular Devices, Sunnyvale, CA; formerly Axon Instruments); macroscopic current data were acquired using Pulse software (HEKA Elektronik, Lambrecht, Germany) with a sampling frequency of 25 kHz, low-pass filtered at 10 kHz and initial pipette resistances were 0.4–0.8 MΩ. From a holding potential of 0 mV, currents were elicited by voltage steps to +80 mV, then to −80 mV, and back to 0 mV. Single-channel recordings were made at 25 kHz sampling rate, low-pass filtered at 1 kHz and initial pipette resistances were 1.5–1.8 MΩ. For both macroscopic and single-channel recordings, the intracellular and extracellular solutions typically contained 130 mM NaCl, 0.2 mM EDTA, and 3 mM HEPES (pH 7.2). The EDTA was withheld from the solutions where indicated (−EDTA). Based on the algorithm in the CHELATOR program,[28] the expected free-calcium concentrations for the different extracellular solutions were as follows: +EDTA, 2.8E $^{-7}$ M; −EDTA, 1E $^{-4}$ M. Previously performed enzyme-kinetic experiments involving A3 homomeric channels and 10 nM MMP9[16] produce the following estimates of maximal MMP9 activities (V_{MAX}) in the presence and absence of chelator (expressed as proteolytic cleavage *events*): +EDTA, 7 ± 2.0 events·μm^{-2}·min^{-1}; −EDTA, 50 ± 15 events·μm^{-2}·min^{-1}. The cyclic nucleotides, cAMP or cGMP (Sigma-Aldrich, St. Louis, MO), were added to intracellular solutions as indicated. The intracellular solution applied to the face of the patch was changed using an RSC-160 rapid solution changer (Molecular Kinetics, Indianapolis, IN). Stock solutions of active human recombinant MMP9 (EMD Millipore, Billerica, MA) were diluted to 1 μg/mL with the extracellular (pipette) solution and added to the patch electrode prior to patch-clamp recording. The MMP stock solutions included 10 mM $CaCl_2$.

For native rod CNG channel recordings, retinas were dissected from *Xenopus laevis* and placed in a frog Ringer's solution: 111 mM NaCl, 2.5 mM KCl, 1 mM $CaCl_2$, 1.2 mM $MgCl_2$, 10 mM D-glucose, 0.2 mM EDTA, and 3 mM HEPES (pH 7.6). Rod outer segments were isolated by gentle mechanical agitation of the retinal tissue and allowed to settle in the

recording chamber (i.e., a non-coated polystyrene tissue culture dish). Patch-clamp experiments were performed in the inside-out configuration as described above. In the event the rods detached from the chamber floor during patch excision (maintaining a "cell attached" configuration), excision was facilitated by gently tapping the pipette electrode holder. Initial pipette resistances were 3–6 MΩ.

Data Analysis

Currents were leak subtracted using the current traces elicited in the absence of cyclic nucleotides before analysis. For channel activation by cGMP dose-response data were fit with the Hill equation: $I/I_{MAX} = [cNMP]^{nH}/(K_{1/2}{}^{nH} + [cNMP]^{nH})$, where I is the current amplitude, I_{MAX} is the maximum current elicited by saturating concentration of ligand, [cNMP] is the ligand concentration, $K_{1/2}$ is the apparent ligand affinity, and n_H is the Hill slope. Fitting with the Hill equation was accomplished with Octave, an open source data-analysis package (www.octave.org), using a custom fitting routine based on *the method of steepest descent*.

For non-stationary fluctuation analysis, mean isochrone current variances across 10 current traces were measured for each cGMP concentration. The cGMP-elicited variances were subtracted by the mean current variance elicited in the absence of cyclic nucleotides. Mean variances were plotted against their respective mean macroscopic current amplitudes and were fit with the parabolic equation: $\sigma^2 = I \cdot i - (I^2/N)$; where σ^2 is the mean current variance, I is the mean macroscopic current amplitude, i is the single-channel current amplitude, and N is the number of conductive channels in the membrane patch.

To quantify the MMP-induced gating effects, the Gibbs free energy of the overall reaction of CNG channel opening (ΔG) was calculated using the equation: $\Delta G = -RT\ ln\ (1/K_{1/2}{}^{nH})$,[29] where R is the gas constant,1.987 $cal \cdot K^{-1} \cdot mol^{-1}$, and T is the temperature in degrees kelvin. The differences of Gibbs free energy change (ΔΔG) caused by MMP activity were calculated: $\Delta\Delta G = \Delta G_{MMP} - \Delta G_{control}$.

Protein biochemistry

Proteolysis experiments for CNGA3 and CNGA1 were performed as previously described.[16] Briefly, *Xenopus* oocytes expressing either FLAG-tagged CNGA3 or FLAG-tagged CNGA1 were exposed either to a mixture of stock MMP9 and MMP2 solutions (100 μg/mL) or an equal volume of MMP vehicle for approximately 1 hour at room temperature prior to sample collection. To potentially facilitate proteolysis, 1 μM CPT-cGMP was added to the reaction solution, exposing the channels to a sub-saturating concentration of cGMP during MMP exposure.[16] Oocyte lysates were prepared as previously described.[27] Briefly, oocytes were placed in lysis buffer containing: 20 mM HEPES (pH 7.5), 150 mM NaCl, 5 mM EDTA, 0.5% Triton X-100 (Thermo Scientific, Rockford, IL) and protease inhibitors (cOmplete, Mini, EDTA-free Protease Inhibitor Cocktail Tablets, Roche Applied Science, Penzberg, Germany). Oocytes were subjected to homogenization and the soluble cell lysate was then separated from yolk and other insoluble material by centrifugation at 20,000 g for 10 min. at 4°C. Lysate representing approximately one oocyte per lane was loaded and separated by SDS-PAGE under reducing conditions on NuPAGE 4–12% Tris acetate gels (Life

Technologies, Carlsbad, CA). Proteins were then transferred to nitrocellulose membrane using the NuPAGE transfer system (Life Technologies). Immunoblots were processed as described previously,[26] FLAG-tagged subunits were detected using an anti-FLAG M2 monoclonal antibody (Sigma-Aldrich) at a concentration of 1:50,000 in TTBS buffer with 1% nonfat dry milk, followed by chemiluminescent detection (SuperSignal West Dura Substrate, Thermo Scientific). The approximate molecular weights of the FLAG-tagged subunits were estimated using protein standards (SeeBlue Plus2, Life Technologies).

Statistical Analysis

ANOVAs, single-pairwise and multiple-pairwise comparisons were performed with NCSS statistical software (NCSS, Kaysville, UT). Data were tested for normality and equal variance prior to hypothesis testing. Data were tested for normality and equal variance prior to hypothesis testing; data which violated the assumption of equal variance were analyzed with the Mann-Whitney test as indicated. Single pairwise comparisons of normally-distributed and equal-variant (NDEV) data were analyzed with the Student's *t*-test; multiple pairwise comparisons of NDEV data were analyzed with the Holm-Bonferroni corrected *t*-test[30] subsequent to statistically significant ANOVA result. A p value less than 0.05 was considered to be statistically significant for all hypothesis tests. All values are reported as the mean ± S.E.M. of n experiments (patches) unless otherwise indicated.

RESULTS

MMP9 enhances ligand sensitivity and decreases maximum current of heteromeric CNGA3 + CNGB3 channels

We examined the effects of MMP9 on CNG channel gating and rundown using inside-out patches excised from *Xenopus* oocytes expressing both CNGA3 and CNGB3 subunits. MMP9 (10 nM) was added to the patch-electrode solution, thus providing access to the extracellular surface of the membrane patch. We assessed CNG channel gating properties by measuring cGMP dose-response relationships, determining the apparent affinity for cGMP using fits with the Hill equation. Since MMP catalytic activity is dependent on association with divalent cations, including Zn^{2+} and Ca^{2+},[31] we examined the MMP-dependent changes in CNG channel activity under both high and low divalent cation concentrations, produced by omitting chelator (−EDTA) or including EDTA (+EDTA) in the extracellular solution; the expected free-calcium concentrations were: −EDTA, 1E $^{-4}$ M; +EDTA, 2.8E $^{-7}$ M (see *Experimental Procedures*). As shown previously,[16] extracellular application of MMP9, in the presence of a low divalent cation concentration, increased the apparent affinity for cGMP (decreased $K_{1/2}$) relative to control patches (Figure 1A,B). Within 20 minutes of MMP exposure, both the $K_{1/2}$ cGMP (mean ± S.E.M; MMP, $K_{1/2}$ = 7.4 μM ± 0.8; Control, $K_{1/2}$ = 15.2 μM ± 1.1; $p < 0.001$, Student's *t*-test, n = 5, 7) and the Hill slope (n_H) (MMP, $n_H = 1.6 \pm 0.2$; Control, $n_H = 2.1 \pm 0.1$; $p < 0.05$, Student's *t*-test, n = 5, 7) were significantly reduced for MMP treated patches. These changes in gating enhanced the current elicited by a subsaturating concentration of cGMP (2 μM) (Figure 1C). We previously demonstrated that high divalent cation concentrations accelerated the MMP dependent gating changes in CNGA3 homomeric (A3) channels.[16] Similarly, we observed that high divalent cation concentrations accelerated MMP9 dependent effects on gating for

CNGA3 plus CNGB3 (A3+B3) heteromeric channels (Figure 1A,B). Within 20 minutes of patch excision, MMP9 in a high concentration of divalent cations effected a more profound reduction in $K_{1/2}$ cGMP ($K_{1/2}$ = 1.5 μM ± 0.2; $p < 0.001$, Student's *t*-test, n = 4, 5) and in the Hill slope (n_H = 0.78 ± 0.07; $p < 0.01$, Student's *t*-test, n = 4, 5) relative to MMP9 in a low concentration of divalent cations. In addition to the changes in channel gating, prolonged exposure to MMP9 promoted a decrease in the maximal cGMP-elicited current (I_{MAX} rundown) that was also accelerated and enhanced by high divalent cation concentrations (Figure 1C,D). Within 40 minutes of patch excision, the MMP treated patches (−EDTA) exhibited considerable I_{MAX} rundown relative to control patches (MMP, $I_{MAX}/I_{MAX,TO}$ = 0.31 ± 0.03; $I_{MAX}/I_{MAX,TO}$ = 0.89 ± 0.04). Taken together, these data suggest that MMP-dependent proteolysis is antecedent to both the enhanced ligand sensitivity and I_{MAX} rundown of A3+B3 heteromeric channels.

MMP-dependent I_{MAX} rundown is due to loss of conductive channels

The macroscopic current amplitude (*I*) is determined by the single channel current (*i*), the number of conductive channels (*N*) and the open probability (P_O), where $I = iNP_O$. Accordingly, MMP exposure may promote I_{MAX} rundown by decreasing the number of conductive channels, the single-channel conductance, or the maximum open probability. In order to distinguish between these possibilities, we analyzed the current-variance relationship of MMP treated A3+B3 heteromeric channels (see *Experimental Procedures*). If the MMP-mediated I_{MAX} rundown is due to a decrease in the maximum open probability, we would expect to see an increase in the current variance at saturating cGMP (as $P_{O,MAX}$ approaches 0.5). However, the current variance in saturating cGMP decreases with I_{MAX} rundown (Figure 2A,B). This decrease in the current variance during I_{MAX} rundown was also observed for A3 homomeric channels (data not shown). The linear relationship between the variance and I_{MAX} rundown is consistent with a decrease in conductive channels.

To further examine the nature of the I_{MAX} rundown, we examined single-channel activity of MMP9 treated A3 channels in the presence of a saturating concentration of cGMP (1 mM). With extended exposure to MMP9, we observed discrete reductions in current equivalent to the estimated single channel current amplitude (mean ± S.D.; Δi = −3.6 pA ± 0.5) (Figure 2C–E). However, MMP exposure did not reduce the estimated single-channel current amplitude (before reduction: i = 3.5 pA ± 0.5; after reduction: i = 3.5 pA ± 0.6; $p > 0.10$, Student's *t*-test, n = 3) or the maximum open probability (before reduction: $P_{O,MAX}$ = 0.97 ± 0.02; after reduction: $P_{O,MAX}$ = 0.99 ± 0.003; $p > 0.1$, Student's *t*-test, n = 3) for the remaining conductive channels. Collectively, these results indicate that the MMP-dependent I_{MAX} rundown is due to a loss of conductive channels (decreased *N*) rather than a decrease in the single channel current amplitude or in the maximum open probability.

CNGA3 N-glycosylation protects against MMP-dependent processing

Intriguingly, we observed a reversal of $K_{1/2}$ cGMP to control levels after extended MMP exposure (40–60 minutes) under conditions of enhanced MMP activity (i.e., high divalent cation concentration). This recovery in $K_{1/2}$ cGMP was observed for both A3+B3 heteromeric (Figure 3A) and A3 homomeric channels (Figure 3B). Due to temporal variation across experiments, we summarized the gating effects by binning $K_{1/2}$ cGMP for

Initial (at time of excision), *Peak* (at maximal gating effect) and approximate *Endpoint* (35 to 20 percent of the *Initial* I_{MAX}). The $K_{1/2,GMP}$ at these binned groups were as follows (mean ± S.E.M): for A3+B3 heteromeric channels, *Initial* = 11.8 μM ± 1.0, *Peak* = 1.2 μM ± 0.1, and *Endpoint* = 10.0 μM ± 2.8 ; for A3 homomeric channels, *Initial* = 5.6 μM ± 1.0, *Peak* = 0.15 μM ± 0.03, and *Endpoint* = 8.6 μM ± 0.6. The changes in $K_{1/2}$ cGMP were accompanied by corresponding changes in cAMP efficacy for both channel compositions (*data not shown*). These results imply a reversion of channel gating properties to control levels (i.e., gating reversion) with extended MMP exposure.

The above results were surprising as we expect proteolytic modification of core channel subunits to irreversibly affect channel function. One possible explanation for these observations is that the apparent gating reversion arises from a subset of the CNG channels being resistant to the MMP-mediated gating changes and eventual loss of conductivity. Accordingly, the loss of MMP-modified channels (underlying I_{MAX} rundown) would increase the relative contribution of the resistant, non-modified channels to the macroscopic current. Human CNGA3 subunits possess a single N-glycosylation site within the pore turret (N339; Figure 4A). Since glycosylation can impart protection against substrate proteolysis,[32–35] we hypothesized that CNGA turret glycosylation confers resistance to MMP-dependent processing. To test this hypothesis, we utilized a CNGA3 mutant lacking the N339 turret glycosylation site ($A3_{N339Q}$). First, we exposed intact oocytes expressing CNGA3 wild type ($A3_{wt}$) or $A3_{N339Q}$ channels to MMPs for 1 hour. With immunoblot analysis we observed a loss of the full-length channel subunits for both the non-glycosylated/core-glycosylated form of the $A3_{wt}$ subunits and the $A3_{N339Q}$ subunits (Figure 4B). Conversely, glycosylated $A3_{wt}$ subunits were relatively resistant to MMP-dependent proteolysis (Figure 4B).

Next, we investigated the effects of MMP exposure on gating and I_{MAX} rundown of $A3_{N339Q}$ channels. We predicted that if pore-turret glycosylation protects against MMP-dependent modifications, then removal of the glycosylation site will reduce or eliminate the protected subpopulation, thereby attenuating the observed gating reversion. Similar to $A3_{wt}$ channels, MMP exposure increased the ligand sensitivity and promoted I_{MAX} rundown of $A3_{N339Q}$ channels. However, even with extensive I_{MAX} rundown, $A3_{N339Q}$ channels did not exhibit an obvious reversal in ligand sensitivity (Figure 4C). To quantitatively compare the extent of the gating reversion between $A3_{wt}$ and $A3_{N339Q}$ channels, we calculated the MMP-dependent changes in the free-energy difference of the channel opening transition ($\Delta\Delta G$; where $\Delta\Delta G = \Delta G_{MMP} - \Delta G_{control}$) for each channel composition (see *Experimental Procedures*). Subsequent to the maximal MMP-dependent change in gating ($\Delta\Delta G \approx -3$ kcal/mol), the $\Delta\Delta G$ for $A3_{wt}$ channels increased to approximately −1 kcal/mol at low $I_{MAX}/I_{MAX,T0}$, signifying a profound gating reversion with extensive I_{MAX} rundown (Figure 4D). In contrast, the $\Delta\Delta G$ for MMP treated $A3_{N339Q}$ channels progressively decreased to approximately −4 kcal/mol at low $I_{MAX}/I_{MAX,T0}$, indicating that the gating reversion was virtually absent for $A3_{N339Q}$ channels (Figure 4D). We observed a similar effect with oocytes expressing $A3_{wt}$ channels that were treated with tunicamycin, an inhibitor of N-glycosylation (*data not shown*). Furthermore, the gating properties and time-dependent changes in I_{MAX} for untreated $A3_{N339Q}$ channels were not significantly different from

untreated $A3_{wt}$ channels (*data not shown*). Collectively, these results suggest that the observed reversion in ligand sensitivity of MMP modified $A3_{wt}$ channels is likely due to the emerging contribution of MMP-resistant channels, and that N-glycosylation within the pore turret confers this resistance.

Position of the CNGA glycosylation site within the pore turret determines whether CNG channels are protected from MMP-dependent modification

Native rod photoreceptor CNG channels are heterotetramers containing CNGA1 and CNGB1 subunits. To characterize the MMP-dependent change in ligand sensitivity and I_{MAX} rundown of rod CNG channels, we examined the effects of MMP9 on expressed bovine CNGA1 homomeric channels (A1) or CNGA1 co-expressed with human CNGB1 (A1+B1). Similar to CNGA3 subunits, CNGA1 subunits possess a single N-glycosylation site within the pore turret.[23] Unlike CNGA3 subunits, immunoblot analysis of FLAG-tagged CNGA1 subunits suggests that the glycosylated and non-glycosylated forms of the subunit are equally susceptible to in vitro MMP9 proteolysis, both in the context of homomeric A1 or heteromeric A1+B1 channels (Figure 5A). Next, we examined the relationship between the MMP mediated I_{MAX} rundown and the apparent gating reversion (i.e. emergence of a protected subpopulation) for A1 channels. In contrast to A3 channels, gating reversion was nearly absent for A1 channels (Figure 5B). For A3 channels, gating reversion is apparent as I_{MAX} approaches ~50% of the initial amplitude and nearly complete reversion is apparent at ~10% of the initial I_{MAX}. However, A1 channels exhibit only a partial reversion at ~10% of the initial I_{MAX} (Figure 5C).

Next we tested whether CNGA1 glycosylation is ineffective at protecting A1+B1 heteromeric channels from the MMP dependent gating changes. We monitored the MMP-dependent changes in gating for patches that contained heterologously expressed A1+B1 channels and patches containing native A1+B1 channels excised from *Xenopus* rod outer segments. Similar to A1 homomeric channels, the heterologously expressed A1+B1 heteromeric channels lacked a distinct gating reversion with I_{MAX} rundown (Figure 5D). Unexpectedly, *Xenopus* rod A1+B1 channels demonstrated a profound gating reversion (Figure 5D), which was comparable to the reversion observed with CNGA3-containing channels (see Figure 3).

Interestingly, protein sequence alignments for the turret region of homologous channel subunits indicate that CNGA glycosylation occurs at two distinct positions within the pore turret: the bovine CNGA1 glycosylation site (*position 1*) is shifted toward the amino terminus in relation to other paralogs and orthologs, including that of *Xenopus* CNGA1 (*position 2*) (Figure 6A). This led us to hypothesize that the location of the glycosylation site within the pore turret determines whether CNG channels are protected from MMP-dependent processing. To test this hypothesis, we utilized a bovine CNGA1 mutant engineered to relocate the glycosylation site to *position 2*, which is the glycosylation site found in human CNGA3 and *Xenopus* CNGA1: N337T, D344N, N346S ($CNGA1_{NDN\text{-}TNS}$) (Figure 6A). In contrast to channels containing wild type CNGA1 subunits, channels containing $CNGA1_{NDN\text{-}TNS}$ subunits exhibited a robust gating reversion following extensive I_{MAX} rundown with MMP exposure (Figure 6B); $A1_{NDN\text{-}TNS}$ channels also

exhibited a reduced maximum change in apparent cGMP affinity compared to $A1_{wt}$ channels ($K_{1/2}$ cGMP at *Peak* of gating effect: $A1_{NDN\text{-}TNS}$, $K_{1/2}$ = 16.1 μM ± 4.3; $A1_{wt}$, $K_{1/2}$ = 3.5 μM ± 1.8; $p < 0.05$, Mann-Whitney test, n = 5). The reduced maximal change in $K_{1/2}$ cGMP for $A1_{NDN\text{-}TNS}$ channels is likely due to an increased contribution of unmodified channels to the macroscopic dose-response relationship. For control (untreated) $A1_{wt}$ channels, the previously characterized increase in ligand sensitivity (run up) associated with tyrosine dephosphorylation[6] was observed (Figure 6B). The NDN-TNS mutations did not alter the gating properties, run up in ligand sensitivity, or time-dependent changes in I_{MAX} for untreated channels (*data not shown*). In our experiments, gating reversion was reduced or eliminated in instances where the glycosylation site was absent ($CNGA3_{N339Q}$) or located at *position 1* (bovine $CNGA1_{wt}$) (Figure 6C). Collectively, these results indicate that the location of the glycosylation site is an important determinant influencing whether CNG channels are protected from MMP-dependent processing.

DISCUSSION

Two contrasting events are associated with MMP-dependent modifications to CNG channels: increased ligand sensitivity and a loss of conducting channels. MMPs are known to have many extracellular and pericellular substrates, making it plausible that MMPs alter CNG channel activity indirectly through other signaling systems (e.g., integrins, ICAM).[36,37] Although we can not rule out indirect contributions to the gating changes, previous experiments indicated that the MMP dependent gating effects likely arise from direct proteolysis of core channel subunits.[16] In accordance with previous observations,[16] these gating effects increased the current in 2 μM cGMP, which is the approximate physiological cGMP concentration in photoreceptors in the dark.[38] Concomitant to the increased ligand sensitivity is a reduction in the Hill slope of cGMP dose-response curves (see Figure 1). Analyses of cGMP dose-response curves and current fluctuations suggest that MMPs generate CNG channel subpopulations by sequentially modifying individual CNGA subunits, where the apparent affinity for cGMP is governed by the total number of modified subunits (from 0 to 4) (Meighan, Meighan and Varnum, unpublished observations). The heterogeneous ligand sensitivities produced by differentially modified CNG channels would cause a reduction in the Hill slope for cGMP dose response curves. Consistent with this, it has been reported previously that heterogeneous gating properties likely accounts for differences in Hill slope between single-channel recordings and macroscopic-current recordings of CNG channels.[39] With prolonged MMP exposure, we observed a reduction in the maximal current. Single-channel recordings and macroscopic current fluctuations indicate that the current loss is apparently due to a loss of conductive CNG channels. This suggests that MMP-processed channels become either non-functional, or enter a non-conductive or persistently-closed state. Based on the temporal relationship between the gating effects and the I_{MAX} rundown, we suspect that the biochemical events producing the loss of conductivity occur subsequent to the proteolytic events underlying the gating change.

For the channels examined here, multiple CNGA subunits are potentially available for processing by MMPs. One possible mechanism for the loss of conductivity is that proteolysis of a critical number of subunits facilitates entry of the channel into a non-conductive state. Another possibility is that the proteolysis underlying the gating

modification may facilitate secondary cleavage events —by MMPs or other endogenous proteases—rendering the channel non-conductive. Sequential processing by multiple proteases has been described previously in other systems. For example, extracellular cleavage of receptor-like protein-tyrosine phosphatases by metalloproteinases is antecedent to intracellular cleavage by presenilin/γ-secretase.[40] Future experiments will be directed towards characterizing the loss of CNG channel conductivity with MMP proteolysis.

The MMP dependent I_{MAX} rundown revealed a subpopulation of channels that were protected from MMP-dependent processing; that protection was dependent on CNGA subunit glycosylation. There are several means by which channel glycosylation may confer resistance to MMP dependent processing. One possibility is that glycosylation induces an allosteric effect, indirectly preventing access to an MMP cleavage site. This seems unlikely since glycosylation does not alter the gating properties of CNG channels in the absence of MMP treatment. Instead, we postulate that CNGA glycosylation sterically hinders access to the MMP cleavage site(s). In other systems, it has been demonstrated that protein glycosylation can inhibit proteolysis and attendant changes to protein function. For example, N-glycosylation interferes with trypsin-mediated digestion of an intestinal anion exchange protein (SLC26A3), consequently promoting its functional expression.[41] In addition, N-glycosylation of glutamate receptor GluR3 subunits interferes with specific cleavage by granzyme B and the subsequent formation of autoimmune products.[42] Depending on the channel type (rod vs. cone) and configuration (homomeric vs. heteromeric), the CNG channels examined here contain 2–4 CNGA subunits per channel. Therefore, each CNG channel likely contains multiple MMP substrates. How might CNGA glycosylation protect against proteolytic modification of CNG channel subunits? We envision two potential mechanisms for protection against MMP-dependent processing. One potential mechanism is that CNGA glycosylation confers resistance on a subunit-by-subunit basis. For the glycosylation sequons of the channels examined here, glycosylation efficiency is expected to vary from ~50% (e.g., human CNGA3) to ~85% (e.g., bovine CNGA1).[43] Based on these efficiencies, it is likely that CNG channels exhibit a range of glycosylations (from 0 to 4 subunits). Therefore, if glycosylation is protective of individual subunits only, protection from MMPs would exist in degrees (depending on the number of glycosylated subunits). Another potential mechanism is that CNGA glycosylation precludes access of MMPs to the extracellular channel face. In this scenario, channels that are incompletely glycosylated (i.e., containing unglycosylated CNGA subunits) may still be protected from MMP-dependent processing. Future experiments may help distinguish between these possible mechanisms.

The location of the CNGA glycosylation site within the pore turret critically determines whether channels are protected from MMP-dependent processing. There is a nearly uniform location for CNGA2 and CNGA3 turret glycosylation at *position 2* (Fig 6A). In contrast, CNGA1 turret glycosylation sites exhibit greater heterogeneity among orthologs: most mammals present *position 1* glycosylation sites in CNGA1; birds, amphibians and reptiles present *position 2* sites; and many fish CNGA1 orthologs entirely lack a turret glycosylation site. For bovine CNGA1, as in other mammalian CNGA1 orthologs, the *position 1* glycosylation site is shifted by 7 amino acids toward the N-terminus relative to the *position 2* site (e.g., human CNGA3 and *Xenopus* CNGA1). Based on a composite model of human

CNGA1 using the crystal structures of KvAP and the Shaker potassium channel Kv1.2 (Protein Data Bank accession nos. 1ORQ and 3LUT, respectively), this shift may dramatically alter the orientation and position of the glycosylation site relative to the other parts of the channel (Figure 6D). Interestingly, the *position 1* glycosylation site is centrally oriented on the pore turret loop, whereas the *position 2* site is tethered more closely to S5. This positional difference would seemingly permit CNGA3 glycosylations to cover a wider area of the channel surface compared to bovine CNGA1 glycosylation—potentially influencing access of MMPs to the channel. Alternatively, the difference in susceptibility to MMP-mediated proteolysis may be due to differences in proximity between CNGA glycosylation sites and a specific MMP cleavage site(s). Possible MMP cleavage sites, for which access might be differentially occluded by *position 2* versus *position 1* glycosylation, include the extracellular S1–S2 loop, and the pore turret itself. Further studies are necessary to fully elucidate the mechanism by which glycosylation protects against MMP-dependent proteolysis.

It has been demonstrated previously that the absence of the CNGA pore-turret glycosylation does not impact the functional properties of CNG channels.[23,24] This is surprising given that pore-turret glycosylation is remarkably conserved across CNG channel paralogs and orthologs (see Figure 6A), and that functionally important pore-turret glycosylation sites have been characterized for several other members of the voltage-gated channel superfamily.[44] For example, interference of pore-turret glycosylation disrupts targeting of HCN2 channels to the plasma membrane,[20] alters capsaicin sensitivity of TRPV1 channels,[21] and decreases the open probability of the inward rectifier potassium channel, ROMK1.[22] How might CNGA pore-turret glycosylation impact CNG channel function in photoreceptors? We speculate that the CNGA glycosylation regulates susceptibility to processing by retinal MMPs, which have been localized within the interphotoreceptor matrix and other regions of the retina.[45–48] Furthermore, differences in the glycosylation position between CNGA1 and CNGA3 observed in mammals may facilitate divergent sensitivities to MMPs for rod and cone photoreceptors. As a caveat, species- and tissue-specific features in protein glycosylation may complicate extrapolation from heterologous expression systems to photoreceptors. It is noteworthy, however, that the relative abundance of protected channels we observed with native rod photoreceptors (from *Xenopus*) was comparable to recombinant channels formed by $CNGA1_{NDN\text{-}TNS}$ subunits (see Figure 6C).

Removal of CNGA3 glycosylation by the N339Q mutation enhanced the susceptibility of CNG channels to MMP-dependent processing. This is observation is relevant, as a variety of pathological conditions are associated with abnormal hypoglycosylation of protein substrates. Two prominent examples are the family of genetic diseases collectively termed congenital disorders of glycosylation (CDG)[49] and Chagas disease (caused by the flagellate protozoan *Trypanosoma cruzi*).[50] These conditions are often accompanied by cardiac conduction anomalies and arrhythmias, which have been linked to the glycosylation state of Na_V channels of the heart sarcolemma.[51] It is currently unknown whether increased exposure of Na_V channels to extracellular proteases is a contributing factor in these disturbances. Furthermore, disorders of hypoglycosylation are associated with visual dysfunction. For example, both phosphomannomutase deficiency (PMM2-CDG) and

dehydrodolichyl diphosphate synthase (DHDDS-CDG) have been causally linked to retinitis pigmentosa (RP).[52,53] Although it is suspected that CDG-associated RP is due, in part, to N-linked glycosylation deficiency in photoreceptors,[53] it is not understood how the attendant hypoglycosylation of protein substrates relates to the photoreceptor degeneration underlying RP. Increased Ca^{2+} influx through hyperactive CNG channels—resulting in photoreceptor cytotoxicity—is thought to be antecedent to several RP variants.[54–56] Considering that MMPs promote increased ligand sensitivity of CNG channels, and that MMP levels are increased in several retinal pathologies[57–60]—including an animal model of RP[61]—we speculate that enhanced MMP-dependent proteolysis of hypoglycosylated CNG channels may contribute to the pathophysiology of CDG-associated RP. Future studies will be directed toward exploring the importance of CNGA glycosylation for photoreceptor function, and the potential connection between CDG-associated RP and MMP-dependent processing of CNG channels.

Acknowledgments

We are grateful to W.N. Zagotta for sharing bovine CNGA1, S.E. Gordon for providing the human CNGB1 construct, and K.-W. Yau for sharing the cDNA clone for human CNGA3. This work was supported by grants from the National Eye Institute (EY12836 to M.D.V. and EY19907 to R.L.B).

Abbreviations

CNG	cyclic nucleotide-gated
MMP	matrix metalloproteinase
ECM	extracellular matrix
cGMP	cyclic guanosine monophosphate
cAMP	cyclic adenosine monophosphate

LITERATURE CITED

1. Craven KB, Zagotta WN. CNG AND HCN CHANNELS: Two Peas, One Pod. Annual Review of Physiology. 2006; 68:375–401.
2. Pifferi S, Boccaccio A, Menini A. Cyclic nucleotide-gated ion channels in sensory transduction. FEBS Lett. 2006; 580:2853–2859. [PubMed: 16631748]
3. Bradley J, Reisert J, Frings S. Regulation of cyclic nucleotide-gated channels. Current Opinion in Neurobiology. 2005; 15:343–349. [PubMed: 15922582]
4. Molday RS. Calmodulin regulation of cyclic-nucleotide-gated channels. Curr Opin Neurobiol. 1996; 6:445–452. [PubMed: 8794100]
5. Rebrik TI, Botchkina I, Arshavsky VY, Craft CM, Korenbrot JI. CNG-Modulin: A Novel Ca-Dependent Modulator of Ligand Sensitivity in Cone Photoreceptor cGMP-Gated Ion Channels. J Neurosci. 2012; 32:3142–3153. [PubMed: 22378887]
6. Molokanova E, Trivedi B, Savchenko A, Kramer RH. Modulation of rod photoreceptor cyclic nucleotide-gated channels by tyrosine phosphorylation. J Neurosci. 1997; 17:9068–9076. [PubMed: 9364053]
7. Gordon SE, Brautigan DL, Zimmerman AL. Protein phosphatases modulate the apparent agonist affinity of the light-regulated ion channel in retinal rods. Neuron. 1992; 9:739–748. [PubMed: 1382474]

8. Muller F, Vantler M, Weitz D, Eismann E, Zoche M, Koch KW, Kaupp UB. Ligand sensitivity of the α2 subunit from the bovine cone cGMP-gated channel is modulated by protein kinase C but not by calmodulin. J Physiol. 2001; 532:399–409. [PubMed: 11306659]
9. Womack KB, Gordon SE, He F, Wensel TG, Lu CC, Hilgemann DW. Do phosphatidylinositides modulate vertebrate phototransduction? J Neurosci. 2000; 20:2792–2799. [PubMed: 10751430]
10. Brady JD, Rich ED, Martens JR, Karpen JW, Varnum MD, Brown RL. Interplay between PIP3 and calmodulin regulation of olfactory cyclic nucleotide-gated channels. Proc Natl Acad Sci USA. 2006; 103:15635–15640. [PubMed: 17032767]
11. Bright SR, Rich ED, Varnum MD. Regulation of human cone cyclic nucleotide-gated channels by endogenous phospholipids and exogenously applied phosphatidylinositol 3,4,5-trisphosphate. Mol Pharmacol. 2007; 71:176–183. [PubMed: 17018579]
12. Dai G, Peng C, Liu C, Varnum MD. Two structural components in CNGA3 support regulation of cone CNG channels by phosphoinositides. J Gen Physiol. 2013; 141:413–430. [PubMed: 23530136]
13. Korenbrot JI. Speed, adaptation, and stability of the response to light in cone photoreceptors: The functional role of Ca-dependent modulation of ligand sensitivity in cGMP-gated ion channels. J Gen Physiol. 2012; 139:31–56. [PubMed: 22200947]
14. Ko GYP, Ko ML, Dryer SE. Circadian Phase-Dependent Modulation of cGMP-Gated Channels of Cone Photoreceptors by Dopamine and D2 Agonist. J Neurosci. 2003; 23:3145–3153. [PubMed: 12716922]
15. Ko GYP, Ko ML, Dryer SE. Circadian Regulation of cGMP-Gated Cationic Channels of Chick Retinal Cones. Neuron. 2001; 29:255–266. [PubMed: 11182096]
16. Meighan PC, Meighan SE, Rich ED, Brown RL, Varnum MD. Matrix metalloproteinase-9 and -2 enhance the ligand sensitivity of photoreceptor cyclic nucleotide-gated channels. Channels. 2012; 6:181–196. [PubMed: 22699690]
17. Varki A. Biological roles of oligosaccharides: all of the theories are correct. Glycobiology. 1993; 3:97–130. [PubMed: 8490246]
18. Spiro RG. Protein glycosylation: nature, distribution, enzymatic formation, and disease implications of glycopeptide bonds. Glycobiology. 2002; 12:43R–56R.
19. Lis H, Sharon N. Protein glycosylation. Structural and functional aspects. Eur J Biochem. 1993; 218:1–27. [PubMed: 8243456]
20. Much B, Wahl-Schott C, Zong X, Schneider A, Baumann L, Moosmang S, Ludwig A, Biel M. Role of subunit heteromerization and N-linked glycosylation in the formation of functional hyperpolarization-activated cyclic nucleotide-gated channels. J Biol Chem. 2003; 278:43781–43786. [PubMed: 12928435]
21. Wirkner K, Hognestad H, Jahnel R, Hucho F, Illes P. Characterization of rat transient receptor potential vanilloid 1 receptors lacking the N-glycosylation site N604. Neuroreport. 2005; 16:997–1001. [PubMed: 15931076]
22. Schwalbe RA, Wang Z, Wible BA, Brown AM. Potassium Channel Structure and Function as Reported by a Single Glycosylation Sequon. J Biol Chem. 1995; 270:15336–15340. [PubMed: 7797521]
23. Rho S, Lee HM, Lee K, Park C. Effects of mutation at a conserved N-glycosylation site in the bovine retinal cyclic nucleotide-gated ion channel. FEBS Lett. 2000; 478:246–252. [PubMed: 10930577]
24. Faillace MP, Bernabeu RO, Korenbrot JI. Cellular Processing of Cone Photoreceptor Cyclic GMP-gated Ion Channels. J Biol Chem. 2004; 279:22643–22653. [PubMed: 15024024]
25. Yu WP, Grunwald ME, Yau KW. Molecular cloning, functional expression and chromosomal localization of a human homolog of the cyclic nucleotide-gated ion channel of retinal cone photoreceptors. FEBS Letters. 1996; 393:211–215. [PubMed: 8814292]
26. Peng C, Rich ED, Varnum MD. Subunit configuration of heteromeric cone cyclic nucleotide-gated channels. Neuron. 2004; 42:401–410. [PubMed: 15134637]
27. Peng C, Rich ED, Thor CA, Varnum MD. Functionally important calmodulin-binding sites in both NH2- and COOH-terminal regions of the cone photoreceptor cyclic nucleotide-gated channel CNGB3 subunit. J Biol Chem. 2003; 278:24617–24623. [PubMed: 12730238]

28. Schoenmakers TJ, Visser GJ, Flik G, Theuvenet AP. CHELATOR: an improved method for computing metal ion concentrations in physiological solutions. BioTechniques. 1992; 12:870–874. 876–879. [PubMed: 1642895]
29. Kusch J, Zimmer T, Holschuh J, Biskup C, Schulz E, Nache V, Benndorf K. Role of the S4–S5 linker in CNG channel activation. Biophys J. 2010; 99:2488–2496. [PubMed: 20959089]
30. Holm S. A simple sequentially rejective multiple test proceedure. Scandinavian Journal of Statistics. 1979; 6:65–70.
31. Okada Y, Nagase H, Harris ED Jr. A metalloproteinase from human rheumatoid synovial fibroblasts that digests connective tissue matrix components. Purification and characterization. J Biol Chem. 1986; 261:14245–14255. [PubMed: 3095317]
32. Loh YP, Gainer H. Evidence that glycosylation of pro-opiocortin and ACTH influences their proteolysis by trypsin and blood proteases. Molecular and Cellular Endocrinology. 1980; 20:35–44. [PubMed: 6254821]
33. Zhu BC, Fisher SF, Pande H, Calaycay J, Shively JE, Laine RA. Human Placental (fetal) Fibronectin: Increased Glycosylation and Higher Protease Resistance Than Plasma Fibronectin. Presence of Polylactosamine Glycopeptides and Properties of a 44-Kilodalton Chymotryptic Collagen-Binding Domain: Difference from Human Plasma Fibronectin. J Biol Chem. 1984; 259:3962–3970. [PubMed: 6423638]
34. Olden K, Pratt RM, Yamada KM. Role of carbohydrate in biological function of the adhesive glycoprotein fibronectin. Proc Natl Acad Sci USA. 1979; 76:3343–3347. [PubMed: 291008]
35. Kasbaoui L, Harb J, Bernard S, Meflah K. Differences in glycosylation state of fibronectin from two rat colon carcinoma cell lines in relation to tumoral progressiveness. Cancer Res. 1989; 49:5317–5322. [PubMed: 2766300]
36. Tian L, Stefanidakis M, Ning L, Van Lint P, Nyman-Huttunen H, Libert C, Itohara S, Mishina M, Rauvala H, Gahmberg CG. Activation of NMDA receptors promotes dendritic spine development through MMP-mediated ICAM-5 cleavage. J Cell Biol. 2007; 178:687–700. [PubMed: 17682049]
37. Michaluk P, Mikasova L, Groc L, Frischknecht R, Choquet D, Kaczmarek L. Matrix metalloproteinase-9 controls NMDA receptor surface diffusion through integrin beta1 signaling. J Neurosci. 2009; 29:6007–6012. [PubMed: 19420267]
38. Pugh EN Jr, Lamb TD. Amplification and kinetics of the activation steps in phototransduction. Biochim Biophys Acta. 1993; 1141:111–149. [PubMed: 8382952]
39. Ruiz M, Brown RL, He Y, Haley TL, Karpen JW. The single-channel dose-response relation is consistently steep for rod cyclic nucleotide-gated channels: implications for the interpretation of macroscopic dose-response relations. Biochemistry. 1999; 38:10642–10648. [PubMed: 10451358]
40. Chow JPH, Fujikawa A, Shimizu H, Suzuki R, Noda M. Metalloproteinase- and gamma-secretase-mediated cleavage of protein-tyrosine phosphatase receptor type Z. J Biol Chem. 2008; 283:30879–30889. [PubMed: 18713734]
41. Hayashi H, Yamashita Y. Role of N-glycosylation in cell surface expression and protection against proteolysis of the intestinal anion exchanger SLC26A3. Am J Physiol, Cell Physiol. 2012; 302:C781–795. [PubMed: 22159084]
42. Gahring L, Carlson NG, Meyer EL, Rogers SW. Granzyme B proteolysis of a neuronal glutamate receptor generates an autoantigen and is modulated by glycosylation. J Immunol. 2001; 166:1433–1438. [PubMed: 11160179]
43. Mellquist JL, Kasturi L, Spitalnik SL, Shakin-Eshleman SH. The Amino Acid Following an Asn-X-Ser/Thr Sequon Is an Important Determinant of N-Linked Core Glycosylation Efficiency. Biochemistry. 1998; 37:6833–6837. [PubMed: 9578569]
44. Cohen DM. Regulation of TRP channels by N-linked glycosylation. Semin Cell Dev Biol. 2006; 17:630–637. [PubMed: 17215147]
45. Plantner JJ, Drew TA. Polarized distribution of metalloproteinases in the bovine interphotoreceptor matrix. Exp Eye Res. 1994; 59:577–585. [PubMed: 9492759]
46. Padgett LC, Lui GM, Werb Z, LaVail MM. Matrix metalloproteinase-2 and tissue inhibitor of metalloproteinase-1 in the retinal pigment epithelium and interphotoreceptor matrix: vectorial secretion and regulation. Exp Eye Res. 1997; 64:927–938. [PubMed: 9301473]

47. Smine A, Plantner JJ. Membrane type-1 matrix metalloproteinase in human ocular tissues. Curr Eye Res. 1997; 16:925–929. [PubMed: 9288454]

48. Plantner JJ, Smine A, Quinn TA. Matrix metalloproteinases and metalloproteinase inhibitors in human interphotoreceptor matrix and vitreous. Curr Eye Res. 1998; 17:132–140. [PubMed: 9523090]

49. Jaeken J. Congenital disorders of glycosylation. Ann N Y Acad Sci. 2010; 1214:190–198. [PubMed: 21175687]

50. Libby P, Alroy J, Pereira ME. A neuraminidase from Trypanosoma cruzi removes sialic acid from the surface of mammalian myocardial and endothelial cells. J Clin Invest. 1986; 77:127–135. [PubMed: 3080470]

51. Montpetit ML, Stocker PJ, Schwetz TA, Harper JM, Norring SA, Schaffer L, North SJ, Jang-Lee J, Gilmartin T, Head SR, Haslam SM, Dell A, Marth JD, Bennett ES. Regulated and aberrant glycosylation modulate cardiac electrical signaling. Proc Natl Acad Sci USA. 2009; 106:16517–16522. [PubMed: 19666501]

52. Jensen H, Kjaergaard S, Klie F, Moller HU. Ophthalmic manifestations of congenital disorder of glycosylation type 1a. Ophthalmic Genet. 2003; 24:81–88. [PubMed: 12789572]

53. Zuchner S, Dallman J, Wen R, Beecham G, Naj A, Farooq A, Kohli MA, Whitehead PL, Hulme W, Konidari I, Edwards YJK, Cai G, Peter I, Seo D, Buxbaum JD, Haines JL, Blanton S, Young J, Alfonso E, Vance JM, Lam BL, Peričak-Vance MA. Whole-Exome Sequencing Links a Variant in DHDDS to Retinitis Pigmentosa. The American Journal of Human Genetics. 2011; 88:201–206. [PubMed: 21295283]

54. Koch S, Sothilingam V, Garcia Garrido M, Tanimoto N, Becirovic E, Koch F, Seide C, Beck SC, Seeliger MW, Biel M, Muhlfriedel R, Michalakis S. Gene therapy restores vision and delays degeneration in the CNGB1(−/−) mouse model of retinitis pigmentosa. Hum Mol Genet. 2012; 21:4486–4496. [PubMed: 22802073]

55. Paquet-Durand F, Beck S, Michalakis S, Goldmann T, Huber G, Muhlfriedel R, Trifunović D, Fischer MD, Fahl E, Duetsch G, Becirovic E, Wolfrum U, van Veen T, Biel M, Tanimoto N, Seeliger MW. A key role for cyclic nucleotide gated (CNG) channels in cGMP-related retinitis pigmentosa. Hum Mol Genet. 2011; 20:941–947. [PubMed: 21149284]

56. Tosi J, Davis RJ, Wang NK, Naumann M, Lin CS, Tsang SH. shRNA knockdown of guanylate cyclase 2e or cyclic nucleotide gated channel alpha 1 increases photoreceptor survival in a cGMP phosphodiesterase mouse model of retinitis pigmentosa. J Cell Mol Med. 2011; 15:1778–1787. [PubMed: 20950332]

57. Plantner JJ, Jiang C, Smine A. Increase in interphotoreceptor matrix gelatinase A (MMP-2) associated with age-related macular degeneration. Exp Eye Res. 1998; 67:637–645. [PubMed: 9990329]

58. Chen YD, Xu X, Xia X, Wu H, Liu K, Zheng Z, Zhu D. MMP9 is involved in glycation end-products induced increase of retinal vascular permeability in rats and the therapeutic effect of minocycline. Curr Eye Res. 2008; 33:977–983. [PubMed: 19085380]

59. Zhang X, Cheng M, Chintala SK. Kainic acid-mediated upregulation of matrix metalloproteinase-9 promotes retinal degeneration. Invest Ophthalmol Vis Sci. 2004; 45:2374–2383. [PubMed: 15223820]

60. Mali RS, Cheng M, Chintala SK. Intravitreous injection of a membrane depolarization agent causes retinal degeneration via matrix metalloproteinase-9. Invest Ophthalmol Vis Sci. 2005; 46:2125–2132. [PubMed: 15914633]

61. Ahuja S, Ahuja P, Caffe AR, Ekstrom P, Abrahamson M, van Veen T. rd1 mouse retina shows imbalance in cellular distribution and levels of TIMP-1/MMP-9, TIMP-2/MMP-2 and sulfated glycosaminoglycans. Ophthalmic Res. 2006; 38:125–136. [PubMed: 16374054]

62. Arnold K, Bordoli L, Kopp J, Schwede T. The SWISS-MODEL workspace: a web-based environment for protein structure homology modelling. Bioinformatics. 2006; 22:195–201. [PubMed: 16301204]

63. Guex N, Peitsch MC. SWISS-MODEL and the Swiss-PdbViewer: an environment for comparative protein modeling. Electrophoresis. 1997; 18:2714–2723. [PubMed: 9504803]

64. Schwede T, Kopp J, Guex N, Peitsch MC. SWISS-MODEL: An automated protein homology-modeling server. Nucleic Acids Res. 2003; 31:3381–3385. [PubMed: 12824332]

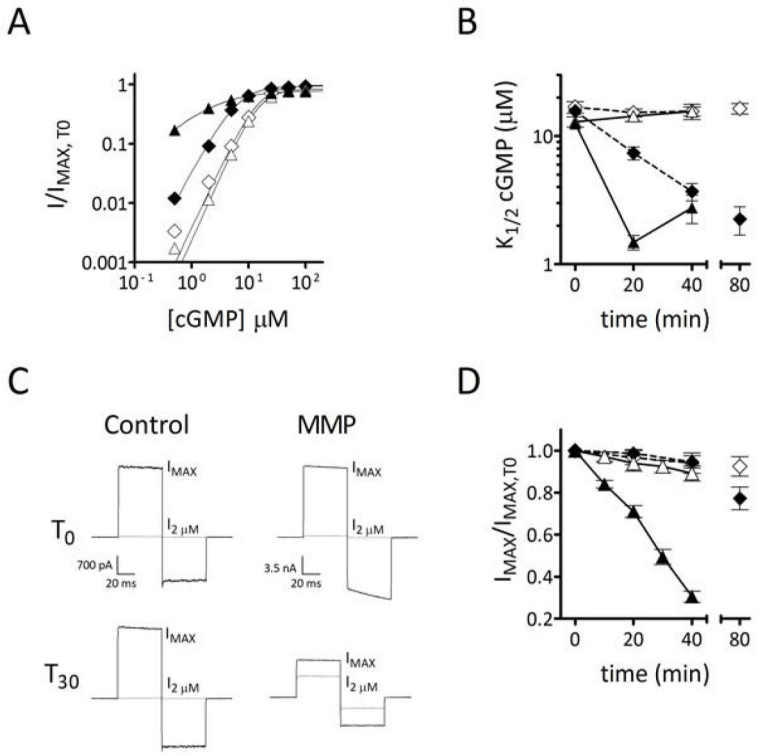

FIGURE 1.

MMP9 enhances ligand sensitivity and decreases maximum current of heteromeric CNGA3 + CNGB3 (A3+B3) channels. **(A)** Representative dose-response relationships for activation of A3+B3 channels by cGMP 20 minutes following excision for control (open) and ~10 nM MMP9-treated (filled) patches. For these recordings, either EDTA (0.2 mM) was present (+EDTA, diamonds) or absent (−EDTA, triangles) in the extracellular solution, thus influencing the availability of free divalents. Currents were measured with an applied voltage of +80 mV, and were normalized to the initial maximum cGMP current (I_{MAX}); currents in the absence of cGMP were subtracted. Continuous curves represent fits using the Hill Equation, as described in *Experimental Procedures*, with the following best-fit parameters: Control +EDTA: $K_{1/2,T20}$ = 15.3 μM, $n_{H,T20}$ = 2.0; MMP +EDTA: $K_{1/2,T20}$ = 6.5 μM, $n_{H,T20}$ = 1.8; Control −EDTA: $K_{1/2,T20}$ = 15.2 μM, $n_{H,T20}$ = 2.2; MMP −EDTA: $K_{1/2,T20}$ = 2.0 μM, $n_{H,T20}$ = 0.9. **(B)** Time course for the change in cGMP apparent affinity for control (open symbols) and MMP-treated (closed symbols) patches following excision. Patch recordings were made either in the presence (diamonds, hashed lines) or absence (triangles, solid lines) of extracellular EDTA. Data were based on best-fit Hill curves and expressed as mean $K_{1/2}$ (± S.E.M). **(C)** Representative current traces for control and MMP9-treated channels (in the absence of EDTA), after activation by a saturating (I_{MAX}, black line) or subsaturating ($I_{2\ \mu M}$, gray line) concentration of cGMP, immediately (top, T_0) and 30 minutes (bottom, T_{30}) following patch excision. Current traces were elicited using voltage steps from a holding potential of 0 mV, to +80 mV, −80 mV, and then returning to 0 mV, and were normalized to the maximum T_0 current. MMP9 increased the current in subsaturating cGMP despite a decrease in maximum current. **(D)** Change in maximum cGMP-elicited current as a function of time following patch excision for control (open

symbols), and MMP9-treated (closed symbols) patches in the presence (diamonds) or absence (triangles) of extracellular EDTA. Currents were normalized to I_{MAX} at time of patch excision ($I_{MAX, T0}$).

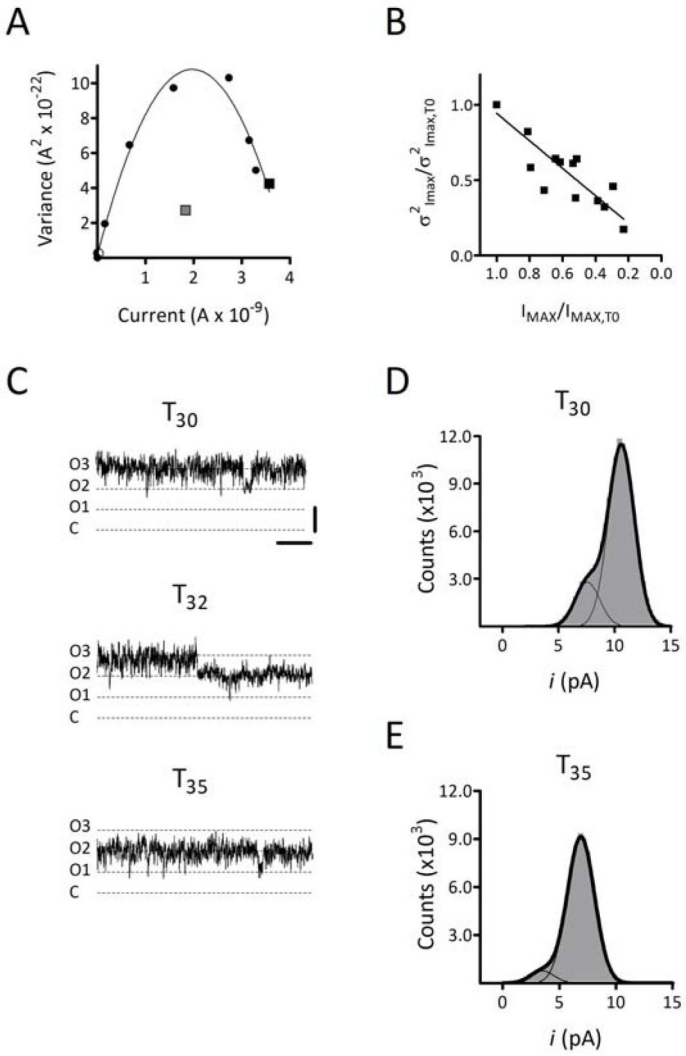

FIGURE 2.

MMP-dependent I_{MAX} rundown is due to loss of conductive channels. **(A)** Representative current-variance relationships for MMP9-treated A3+B3 channels immediately following excision (T_0, black symbols) and ~30 minutes following excision (T_{30}, gray symbol). The black line was produced by fitting the T_0 current-variance data with a 2nd order polynomial (see *Experimental Procedures*). Squares denote the current and variance at a saturating concentration of cGMP (σ^2_{IMAX}) for T_0 and T_{30}. Note the divergence along the vertical axis between the T_{30} σ^2_{IMAX} (gray square) and the predicted curve. **(B)** Regression analysis between the change in I_{MAX} ($I_{MAX}/I_{MAX,TO}$) and the change in the I_{MAX} current variance ($\sigma^2_{IMAX}/\sigma^2_{IMAX,TO}$) for MMP treated A3+B3 channels. Data were pooled from three independent time courses for MMP treated A3+B3 channels (−EDTA). Current variance in saturating cGMP decreases linearly with I_{MAX} rundown (slope = 0.91 ± 0.1, *F* test: $p < 0.001$, n = 15); note the inverted X-axis. **(C)** Representative traces are shown for an inside-out patch containing three CNGA3-only (A3) channels in a saturating concentration of cGMP (1 mM) at ~30 minutes (T_{30}; top), ~32 minutes (T_{32}; middle) and ~35 minutes (T_{35};

bottom) following patch excision. Currents were recorded at a membrane potential of +80 mV. *C*, closed channel mean current level; *O*, current level(s) for open channel(s). Horizontal and vertical scale bars denote 50 ms and 5 pA, respectively. The T_{32} current trace exhibits a persistent loss in current amplitude approximately equal to the unitary current. Current-amplitude histograms for T_{30} **(D)** and T_{35} **(E)** time points were amassed from 4–6 s of recording and fit with the sum of two Gaussian functions. The best-fit Gaussian curves produced the following maximum open probabilities ($P_{O,MAX}$), maximum collective current (I_{MAX}), and single-channel current amplitude (*i*) estimates: T_{30}, $P_{O,MAX}$ = 0.94, I_{MAX} = 10.6 pA, *i* = 3.5 pA; T_{35}, $P_{O,MAX}$ = 0.98 I_{MAX} = 6.9 pA, *i* = 3.5 pA. These results are representative of three independent patches.

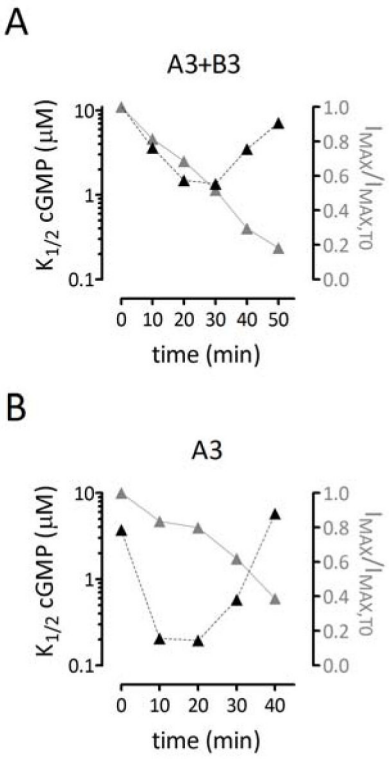

FIGURE 3.

Enhanced MMP-dependent processing of channels produces a gating reversion concomitant with I_{MAX} rundown. Representative time courses are shown for the MMP-dependent change in apparent cGMP affinity of MMP treated heteromeric A3+B3 **(A)** and homomeric A3 channels **(B)**. Data were collected in the absence of extracellular EDTA. For each plot, $K_{1/2}$ cGMP (black triangles, left axis) and I_{MAX} relative to T_0 I_{MAX} (gray triangles, right axis) are shown.

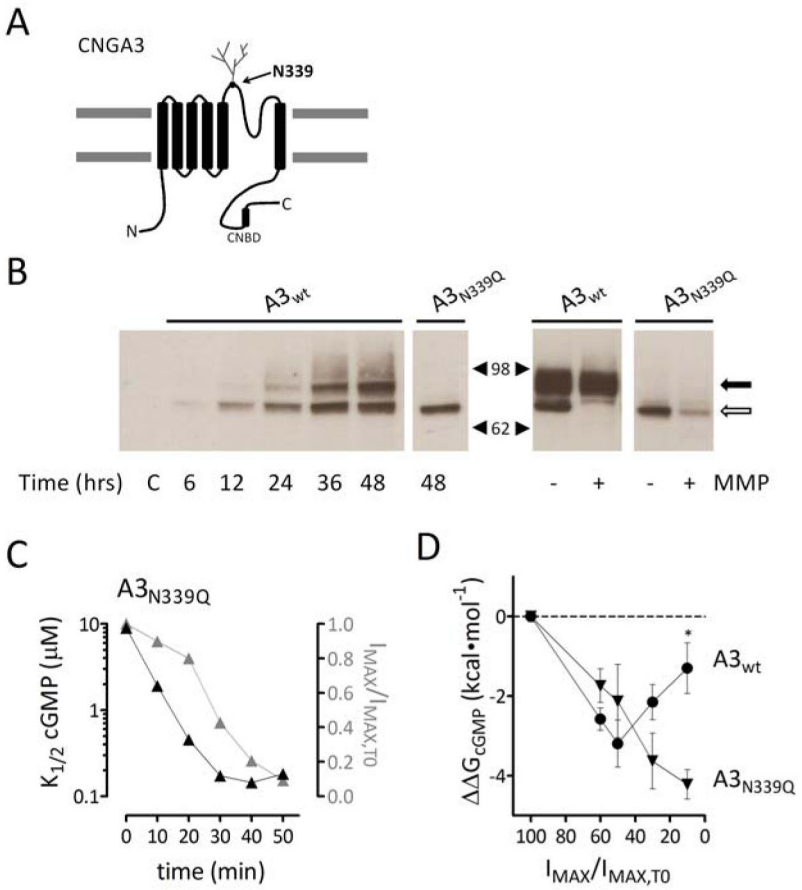

FIGURE 4.

Elimination of CNGA3 N-glycosylation diminishes the gating reversion. **(A)** CNGA3 subunits contain one core N-glycosylation site (N339), which is located in the pore turret; CNBD, cyclic nucleotide binding domain. **(B)** Protein glycosylation can be protective against proteolytic modification by MMP. Immunoblot analysis of protein lysates from oocytes expressing FLAG-CNGA3$_{wt}$ or FLAG-CNGA3$_{N339Q}$ subunits. Time course for expression of glycosylated (filled arrow) and non-glycosylated/core-glycosylated (open arrow) CNGA3 subunits (*left*), and of *in vitro* A3$_{wt}$ and A3$_{N339Q}$ subunit proteolysis by MMPs (*right*); *C*, control uninjected oocytes. Protein immunoreactivity was assessed using anti-FLAG antibody. For in vitro proteolysis experiments, intact oocytes were treated with MMP2 and -9 (100 μg/mL total) for 1-hour, approximately 4-days following mRNA injection. **(C)** Representative time course for the MMP-dependent change in $K_{1/2}$ cGMP (black triangles, left axis) and I_{MAX} (gray triangles, right axis) for A3$_{N339Q}$ channels in the absence of EDTA in the electrode solution (−EDTA). **(D)** Summary of MMP effects on the change in free energy difference for channel gating ($\Delta\Delta G_{cGMP}$, see *Experimental Procedures*) relative to I_{MAX} rundown for A3$_{wt}$ (circles) and A3$_{N339Q}$ (triangles) channels. All recordings were made in the absence of EDTA. $\Delta\Delta G_{cGMP}$ values were binned at various levels of the fractional change in I_{MAX}. The rebound in ligand sensitivity was significantly reduced for A3$_{N339Q}$ compared to A3$_{wt}$ (*p < 0.05, Student's t-test, n = 7).

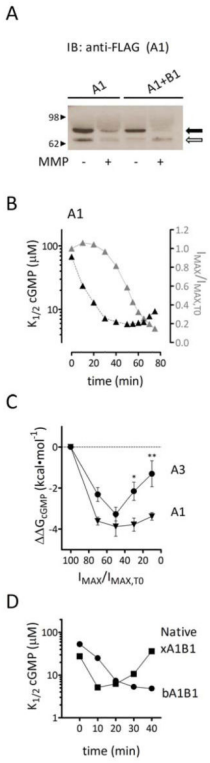

FIGURE 5.

CNGA1 N-glycosylation is only nominally protective against MMP-dependent subunit proteolysis and gating effects. **(A)** Immunoblot analysis of FLAG-tagged CNGA1 (A1) subunits suggests that the glycosylated (filled arrow) and non-glycosylated/ core-glycosylated (open arrow) forms of the subunit are both susceptible to *in vitro* MMP proteolysis, in the context of either homomeric A1 or heteromeric A1+B1 channels. Protein immunoreactivity was assessed using anti-FLAG antibody, and intact oocytes were treated as described in Figure 4B. **(B)** Representative time course for the MMP-dependent change in apparent cGMP affinity (black triangles, left axis) and I_{MAX} (gray triangles, right axis) of A1 homomeric channels. **(C)** Summary of MMP effects on the $\Delta\Delta G_{cGMP}$ in relation to I_{MAX} for A1 and A3 homomeric channels. The rebound in ligand sensitivity was significantly reduced for A1 channels compared to A3 channels (*$p < 0.05$, **$p < 0.01$ Holm's *t*-test, n = 5–13). **(D)** Representative time courses for the change in $K_{1/2}$ cGMP for patches with heterologously expressed A1+B1 channels (comprised of bovine CNGA1 and human CNGB1 subunits) and patches containing native A1+B1 channels excised from *Xenopus* rod outer segments. Native *Xenopus* channels exhibited a pronounced gating reversion with extensive I_{MAX} rundown ($I_{MAX}/I_{MAX,T0} \approx 0.25$ at the conclusion of the time course for both representative patches; MMP-dependent changes in I_{MAX} not shown for clarity).

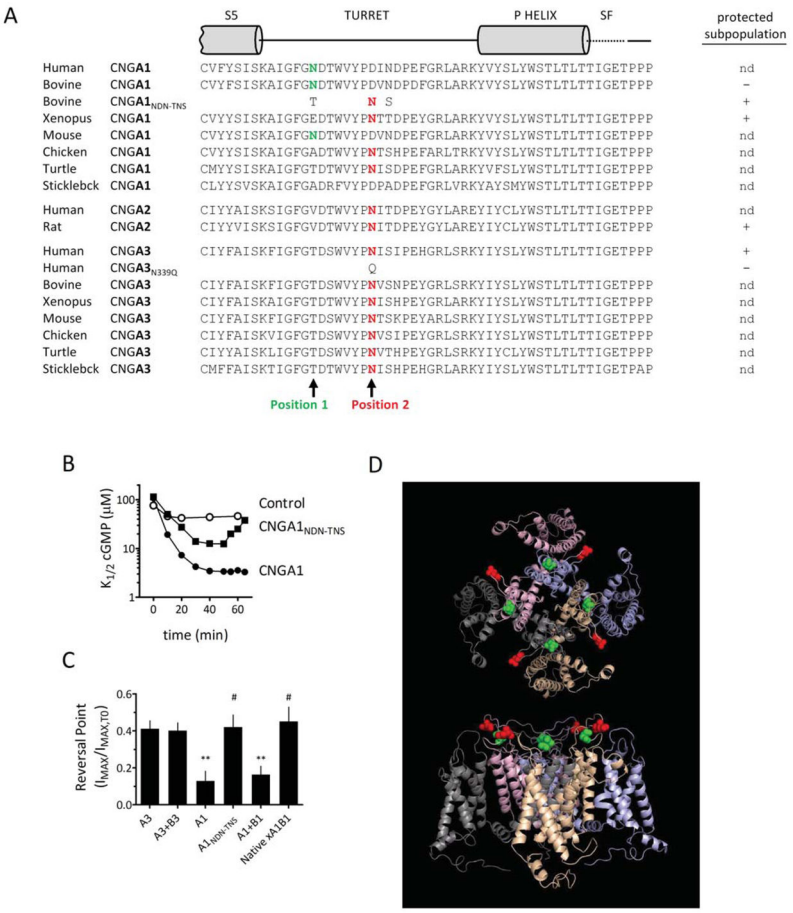

FIGURE 6.

Location of the glycosylation site within the pore turret determines whether CNG channels are protected from MMP-dependent processing. **(A)** Sequence alignment for various CNGA subtypes. Location of conserved N-glycosylation sites in bold. Homomeric channels comprised of rat CNGA2 subunits exhibit a gating reversion comparable to channels comprised of human CNGA3 subunits (data not shown). A "+" indicates substantial fraction of protected channels; "−" indicates limited presence of protected channels; "nd" indicates that the presence of protected channels has not been determined. The accession or entry numbers for the sequences shown are as follows: for CNGA1, NP000078.2 (*Homo sapiens*), NP776703.1 (*Bos taurus*), AAH93579.1 (*Xenopus laevis*), NP031749.2 (*Mus musculus*), NP990551.1 (*Gallus gallus*), K7FWR1 (*Pelodiscus sinensis*), G3N531 (*Gasterosteus aculeatus*); for CNGA2, NP005131.1 (*Homo sapiens*), NP037060.1 (*Rattus norvegicus*); for CNGA3, NP001289.1 (*Homo sapiens*), NP776704.1 (*Bos taurus*), XP004911865.1 (*Xenopus tropicalis*), NP034048.1 (*Mus musculus*), NP990552.1 (*Gallus gallus*), K7GE18 (*Pelodiscus sinensis*), G3PKL4 (*Gasterosteus aculeatus*). **(B)** Representative time courses for the change in $K_{1/2}$ cGMP for channels containing bovine $CNGA1_{wt}$ (control: open circles; MMP-treated: filled circles) and a bovine CNGA1 mutant constructed to move the glycosylation site (*position 1*) to a site homologous to the human CNGA3 glycosylation site: N337T, D344N, N346S ($CNGA1_{NDN\text{-}TNS;}$ filled squares) (*position 2*). Channels comprised of $CNGA1_{NDN\text{-}TNS}$ exhibited a pronounced gating reversion with extensive I_{MAX} rundown

($I_{MAX}/I_{MAX,T0} \approx 0.2$ at the conclusion of the time course for both MMP-treated patches; MMP-dependent changes in I_{MAX} not shown for clarity). **(C)** Extent of I_{MAX} rundown, relative to T_0 I_{MAX}, necessary for the onset of the gating reversion (i.e., I_{MAX} reversal point). Homomeric and heteromeric channels comprised of bovine CNGA1 required a greater extent of I_{MAX} rundown to exhibit a gating reversion (i.e., a reduced I_{MAX} reversal point) compared to channels comprised of human CNGA3 ($p < 0.0001$, single-factor ANOVA; $^{**}p < 0.01$, Holm's *t*-test, n = 5–10) and *Xenopus* CNGA1 ($^{\#}p < 0.05$, Holm's *t*-test, n = 5–6). A reduced I_{MAX} reversal point for bovine $CNGA1_{wt}$-containing channels reflects a less abundant protected population relative to CNGA3-containing channels. Furthermore, repositioning the bovine CNGA1 glycosylation site to a position homologous with the human CNGA3 site increased the relative abundance of protected channels, as evidenced by the elevated I_{MAX} reversal point for $A1_{NDN\text{-}TNS}$ channels relative to $A1_{wt}$ channels ($^{\#}p < 0.05$, Holm's *t*-test, n = 5–6). **(D)** Model of CNG channel structure (S1–S6) showing the relative positions of bovine CNGA1 (*position 1*) versus CNGA3 (*position 2*) glycosylation sites. Human CNGA1 model is viewed from the extracellular side of the membrane (*top*), and through the plane of the membrane, with the extracellular region above and the cytoplasmic region below (*bottom*). The spheres represent the positions of asparagine residues within the glycosylation sequons for *position 1* (green) and *position 2* (red). The S5–S6 segments of CNGA1 were rendered using the crystal structure of KvAP and SWISS-MODEL [62–64] (PDB accession no. 1ORQ). The rendered S5–S6 was subsequently docked to the crystal structure of S1–S4 of the Shaker potassium channel Kv1.2 (PDB accession no. 3LUT) in Pymol. The Kv1.2 S1–S2 linker was altered to match the length of the CNGA1 S1–S2 linker.